REFSANS

Horizontal time-of-flight reflectometer with GISANS option

G. Mangiapia, S. Busch, M. Haese, N. Zec, J.-F. Moulin
German Engineering Material Science Centre at
Heinz Maier-Leibnitz Zentrum
Helmholtz-Zentrum Hereon

GEMS

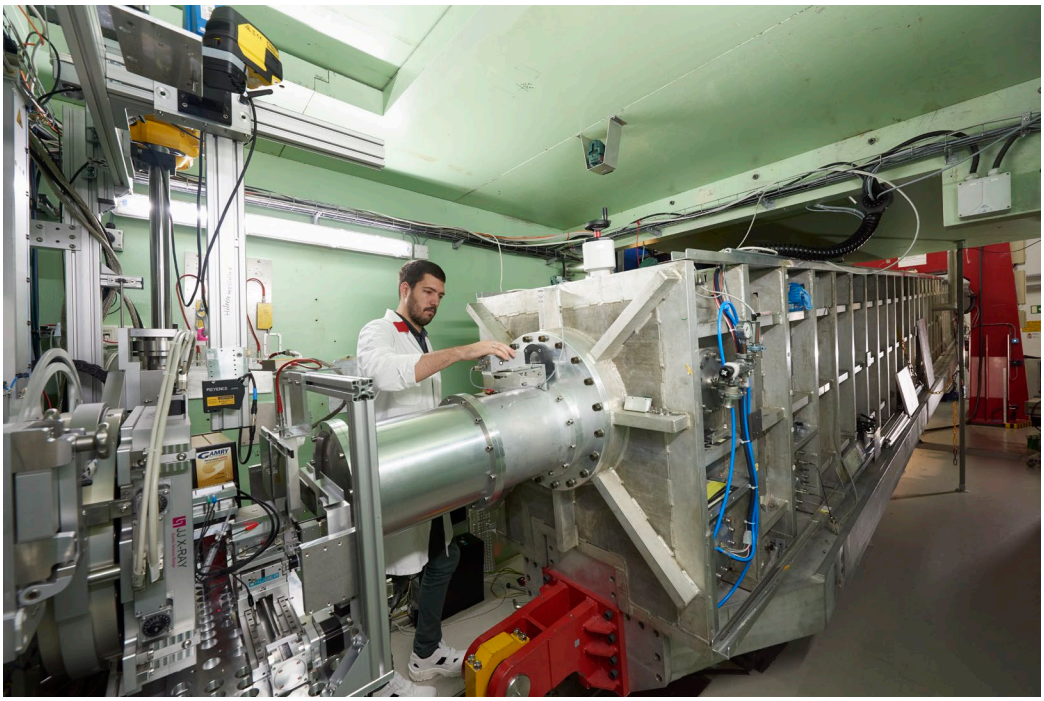

© W. Schürmann / TUM

MLZ
Heinz Maier-Leibnitz Zentrum

Helmholtz-Zentrum
hereon

Contents

1 Introduction

This tutorial will help you to carry out a neutron reflectivity experiment [1] at the horizontal TOF reflectometer REFSANS, installed at the Heinz Maier-Leibnitz Zetrum (MLZ). [2] Neutron reflectivity is a technique belonging to the broader family of neutron scattering techniques. [3-4]

Generally, the aim of scattering experiments is to obtain information either on the structure or on the dynamics of the system under investigation. The systems that can be studied range from crystals to colloidal systems, from proteins to nanostructures. Similarly to microscopy techniques (which study systems in direct space), the spatial resolution of scattering techniques (which probe systems in reciprocal space) is somehow limited by the wavelength of the radiation used. Since in neutron scattering experiments the wavelength ranges roughly from 1 to 25 Å, it is apparent how these experiments are able to provide access at the nanoscale level.

As mentioned, the experiment we are going to perform involves neutron reflectivity. In such an experiment, we are interested in obtaining structural characteristics of a sample, and in particular of its interfaces. Below, we will briefly introduce the basic principles of the technique and then move on to the description of the instrument and the experiment that will be carried out. There are some questions to answer before the experiment, in order to understand the quantities that play a fundamental role in the technique.

For the experiment, you will install the sample together with the instrument scientist, and prepare the instrument in order to start the measurement. Finally, the data will be evaluated and interpreted.

2 Basics

2.1 Background: the neutron source

To carry out neutron experiments, a suitable and reliable neutron source has to be present. Currently, there are two main sources: spallation sources, and reactor sources. [5] In a spallation source a target metal like Mercury, Tantalum or Lead is bombarded by a beam of protons coming from an accelerator: after each impact, a certain number of neutrons is "evaporated" from the heavy nuclei. An important feature in this process is that, due to the pulsed nature of the incident proton beam, the neutron beam is also pulsed over time.

The neutron source used at MLZ falls into the second type of source: a reactor (known as FRM II at MLZ) where $^{235}_{92}\mathrm{U}$ nuclei, contained in a cylindrical rod (*fuel element*), capture a thermal neutron and thereby become unstable. The nuclei split and, among others, emit from two to three very fast neutrons.

The neutrons ejected are too fast and cannot be used to sustain the reaction produced: they have to be slowed down (moderated) at temperatures close to the room temperature (300 K) in order to initiate a new fission. One neutron is used to continue the nuclear chain, while the others can be used for the neutron scattering experiments. The neutrons produced and moderated in the way described are called *thermal* and have a wavelength between 0.5 and 5 Å. For many other experiments, including those of reflectometry, a different range with larger wavelength values is necessary: this is only possible if the neutrons are further slowed down. At this aim a small tank containing liquid deuterium at $\cong$20 K is installed close to the fuel element. From this tank several neutron guides lead the neutrons to the various instruments: the wavelength range of these neutrons (*cold neutrons*) ranges from 1 to 25 Å and is suitable to carry out many experiments, including reflectivity. In any case, differently from what happens in spallation sources, uranium fission produces an almost constant flow of neutrons over time.

2.2 Neutron-nucleus interaction

On general basis, a scattering experiment consists in sending a beam of particles (neutrons) on a target (sample) and studying their diffusion in various directions of space (*i.e.* at various angles). What is essential is that the scattering phenomenon is based on the interaction between neutrons and atomic nuclei, differently from X-rays that interact with electrons. Such interactions can only be described within the quantum mechanics framework. We will briefly sketch the essential details of the neutron-nucleus scattering event. To go further, we will assume the neutron-nucleus interactions as elastic, *i.e.* the energy of the neutron does not change in consequence of the impact. This hypothesis is well fulfilled in reflectivity experiments as the cold neutron energy is too small to excite resonances of the possible scattering nuclei.

Figure 1 shows the scattering of a single neutron from a single nucleus. The incident neutron, far from the nucleus, can be described by a plane wave, whose wavefunction $\psi_{inc}\left(\vec{r}\right)$ is:

$$\psi_{inc}\left(\vec{r}\right) = \psi_0 \exp\left(i\vec{k_i} \cdot \vec{r}\right)$$

where $\vec{k_i}$ is the wave vector of the incident neutron [1], and ψ_0 a constant connected to the incident flux Φ_0 of the beam ($\Phi_0 \propto \left|\psi_0\right|^2$). Once the neutron has been diffused by the nucleus, since we assumed an elastic event, the wave vector $\vec{k_f}$ of the scattered neutron has the same magnitude of $\vec{k_i}$, although a different direction. What is essential to highlight is that the neutron-nucleus interaction occurs only at an extremely small distance from the nucleus (10^{-15}m), much smaller than the wavelength of the cold neutrons used (which always exceeds 1 Å): consequently, nuclei act as point-like scatters, emitting isotropic spherical waves, whose wavefunction $\psi_{sc}\left(\vec{r}\right)$ can be expressed as:

[1] In physics the wave vector $\vec{k}$ is a vector relative to a wave, which has as module the quantity $2\pi/\lambda$, where λ is the radiation wavelength, and as direction that of the wave propagation.

$$\psi_{sc}\left(\vec{r}\right) = -b\frac{\psi_0}{r}\exp\left(ikr\right) \tag{1}$$

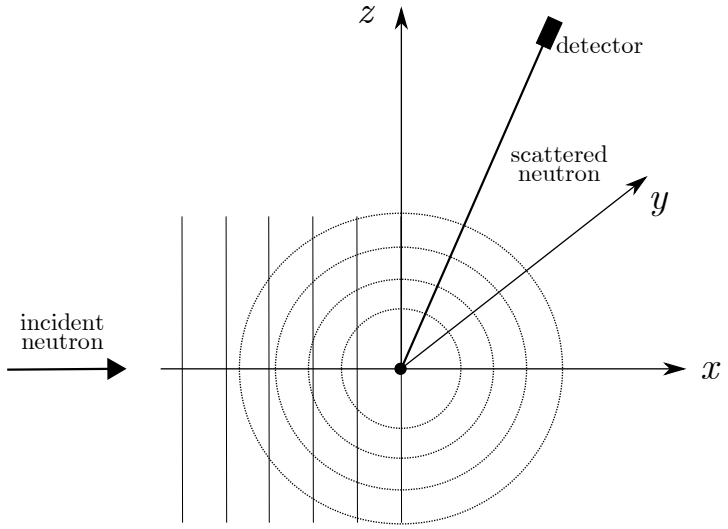

Figure 1 – Neutron scattering geometry from a single nucleus, placed at the origin of the coordinate system. The incident neutron has a plane wavefront, whereas after the interaction it propagates with a spherical wavefront. The detector is set far from the origin.

As the scattering is isotropic, the wave function only depends on the distance from the nucleus. In this equation $k = \left|\vec{k}_i\right| = \left|\vec{k}_f\right|$ is the magnitude of the wave vector; the factor ψ_0/r assures that the total neutron flux is independent of r and is proportional to the incident flux.

In Equation (1) the term b is a constant which describes the "strength" of the nucleus-neutron interaction and is called *scattering length*: it depends on the nucleus (in particular is much different among the different possible isotopes of a certain element), the spin state and is independent within wide limits of the energy of the incident neutron. The minus sign is purely conventional and is used to make most of the nuclei have a positive value of b . [2]

For a real sample, composed by an assembly of particles (nuclei), the wave function of the scattered neutron is just the superimposition of the spherical waves coming from the different nuclei:

$$\psi_{sc}\left(\vec{r}\right) = -\sum\nolimits_j b_j \frac{\psi_0 \exp\left(i\vec{k}_i \cdot \vec{R}_j\right)}{\left|\vec{r} - \vec{R}_j\right|}\exp\left[i\vec{k}_f\left(\vec{r} - \vec{R}_j\right)\right] \tag{2}$$

[2] In the following we will assume for simplicity that the scattering length is real. This is always the case except when the neutron can be absorbed by the nucleus, which we do not deal with.

where the summation is extended over all the nuclei composing the sample. Provided that the nuclei are not located at the origin of the coordinate system, $\vec{r}$ is replaced by $\vec{r} - \vec{R}_j$, $\vec{R}_j$ being the position of the j-th nucleus. It is, on the other hand, easy to verify that Equation (2) is reduced to Equation (1) for a single nucleus.

It is important to observe that by writing the wave function of the scattered neutron as a simple superposition of the spherical waves generated by each nucleus, we are tacitly assuming that a neutron can undergo a single scattering event or that, in other words, a neutron diffused by a certain nucleus does not experience a further scattering event by another nucleus. This approximation is known in the theory of neutron scattering as *first-order Born approximation* and, as said, ignores any so-called *multiple scattering* phenomenon.

The probability to observe a neutron scattered in a certain direction is proportional to the square modulus of $\psi_{sc}\left(\vec{r}\right)$:

$$\left|\psi_{sc}\left(\vec{r}\right)\right|^2 = \left|\sum\nolimits_j b_j \frac{\psi_0 \exp\left(i\vec{k_i}\cdot\vec{R}_j\right)}{\left|\vec{r}-\vec{R}_j\right|}\exp\left[i\vec{k_f}\cdot\left(\vec{r}-\vec{R}_j\right)\right]\right|^2 =$$

$$= \left|\psi_0 \exp\left(ikr\right)\sum\nolimits_j b_j \frac{\exp\left(-i\vec{Q}\cdot\vec{R}_j\right)}{\left|\vec{r}-\vec{R}_j\right|}\right|^2$$

where we have defined the new vector

$$\vec{Q} = \vec{k_f} - \vec{k_i} \tag{3}$$

which play a fundamental role in the theory of neutron scattering processes and is called *scattering vector* or *momentum transfer vector*. A very useful approximation to the formula obtained for $\left|\psi_{sc}\left(\vec{r}\right)\right|^2$ comes from the fact that the sample-to-detector distance, where the neutron is detected, is much larger than the typical sample size. Consequently, to a very good extent, $\vec{r} - \vec{R}_j \cong \vec{r}$ and:

$$\left|\psi_{sc}\left(\vec{r}\right)\right|^2 \cong \left|\psi_0 \sum\nolimits_j b_j \frac{\exp\left(-i\vec{Q}\cdot\vec{R}_j\right)}{r}\right|^2 = \frac{\left|\psi_0\right|^2}{r^2}\left|\sum\nolimits_j b_j \exp\left(-i\vec{Q}\cdot\vec{R}_j\right)\right|^2 =$$

$$= \frac{\left|\psi_0\right|^2}{r^2}\sum\nolimits_j \sum\nolimits_k b_j b_k \exp\left[-i\vec{Q}\cdot\left(\vec{R}_j - \vec{R}_k\right)\right] \tag{4}$$

The last expression in Equation (4) catches the essential characteristic of a neutron scattering experiment: the intensity recorded in a certain direction depends on the superimposition of the spherical waves generated by the assembly of nuclei: if there is a correlation between their positions, the correlation will give rise to constructive interference that will result in maxima of intensity along some directions.

2.3 Coherent and incoherent scattering

As mentioned in Paragraph 2.2, the scattering length is different for different isotopes of a given element, as well as varying for different nuclear spin states. When Equation (4) is applied, it is necessary to consider that the different isotopes of a given element are normally randomly distributed over all sites. The nuclear spin orientation is also randomly distributed, except in special cases such as at very low temperatures.

Consequently, Equation (4) has to be averaged over the random distribution of the scattering length in the sample. If we use the brackets $\langle\ \ \rangle$ to indicate such an average, Equation (4) can be written as:

$$\left|\psi_{sc}\left(\vec{r}\right)\right|^2 = \frac{\left|\psi_0\right|^2}{r^2}\left\langle \sum_j \sum_k b_j b_k \exp\left[-i\vec{Q}\cdot\left(\vec{R}_j - \vec{R}_k\right)\right]\right\rangle$$

If we assume no correlation between positions $\vec{R}$ and b values, the average on the whole double sum is reduced to the average on the values of $b_j b_k$:

$$\left|\psi_{sc}\left(\vec{r}\right)\right|^2 = \frac{\left|\psi_0\right|^2}{r^2}\sum_j \sum_k \left\langle b_j b_k \right\rangle \exp\left[-i\vec{Q}\cdot\left(\vec{R}_j - \vec{R}_k\right)\right]$$

Since the distribution of the scattering lengths on the different positions is uncorrelated, when $j \neq k$, the expectation value of the product $\left\langle b_j b_k \right\rangle$ is equivalent to the product of the expectation values $\left\langle b_j \right\rangle\left\langle b_k \right\rangle$. On the other hand, when $j = k$ we have, after easy transformations:

$$\left\langle b_j b_j \right\rangle = \left\langle b_j^2 \right\rangle = \left\langle b_j \right\rangle^2 + \left\langle \left(b_j - \left\langle b_j \right\rangle\right)^2 \right\rangle$$

Thus, last equation we obtained for $\left|\psi_{sc}\left(\vec{r}\right)\right|^2$ can be rearranged as:

$$\begin{aligned}\left|\psi_{sc}\left(\vec{r}\right)\right|^2 = \frac{\left|\psi_0\right|^2}{r^2}\Bigg\{ &\sum_j \sum_k \left\langle b_j \right\rangle\left\langle b_k \right\rangle \exp\left[-i\vec{Q}\cdot\left(\vec{R}_j - \vec{R}_k\right)\right] + \\ &+ \sum_l N_l \left\langle \left(b_l - \left\langle b_l \right\rangle\right)^2 \right\rangle \Bigg\}\end{aligned} \tag{5}$$

From Equation (5) we see that the scattering intensity, proportional to $\left|\psi_{sc}\left(\vec{r}\right)\right|^2$, is the contribution of two terms. The first term is a sum over all the nuclei and contains the phase factors $\exp\left[-i\vec{Q}\cdot\left(\vec{R}_j - \vec{R}_k\right)\right]$ coming from the superposition of spherical waves generated from the nuclei: this term contains the structural properties of the sample and takes into account interference effects and is called *coherent scattering*. On the other hand, the second term is the standard deviation over the different species (elements) composing the sample (each of which has N_l nuclei in the sample) and does not show neither a dependence on the direction identified by the vector $\vec{Q}$ nor a phase information: this term contains scattering lengths averaged over the isotope- and nuclear spin-distribution of a given element and is called *incoherent scattering*.

Since the neutron has an intrinsic spin of $I_n = 1/2$, if we want to apply Equation (5) to the proton, *i.e.* the nucleus of ${}^1_1\mathrm{H}$ which has a nuclear spin of $I_{{}^1_1\mathrm{H}} = 1/2$, we have to consider two different values for the total spin state: $I_n + I_{{}^1_1\mathrm{H}} = 1$, with a multiplicity of $2 \cdot 1 + 1 = 3$ and $\left| I_n - I_{{}^1_1\mathrm{H}} \right| = 0$, with a multiplicity of $2 \cdot 0 + 1 = 1$ [6] which we will indicate as spin $(+)$ and $(-)$, respectively. Since it has been experimentally determined that $b_{(+)} = 1.0851 \cdot 10^{-4}\,\text{Å}$ and $b_{(-)} = -4.7517 \cdot 10^{-4}\,\text{Å}$, we get:

$$b_{{}^1_1\mathrm{H}}^{(coh)} = \left\langle b_{{}^1_1\mathrm{H}} \right\rangle = \frac{3}{4} b_{(+)} + \frac{1}{4} b_{(-)} = -3.741 \cdot 10^{-5}\,\text{Å}$$

$$\begin{aligned} b_{{}^1_1\mathrm{H}}^{(incoh)} &= \sqrt{\left\langle \left(b_{{}^1_1\mathrm{H}} - \left\langle b_{{}^1_1\mathrm{H}} \right\rangle \right)^2 \right\rangle} = \sqrt{\left[\frac{3}{4} \left(b_{(+)} - \left\langle b_{{}^1_1\mathrm{H}} \right\rangle \right)^2 + \frac{1}{4} \left(b_{(-)} - \left\langle b_{{}^1_1\mathrm{H}} \right\rangle \right)^2 \right]} = \\ &= 2.5274 \cdot 10^{-4}\,\text{Å} \end{aligned}$$

The incoherent scattering length is among the largest of all isotopes and makes hydrogen a big incoherent scatterer, a feature which is used in studies on the dynamics of hydrogenated materials, including biological systems. In reflectivity studies, where we are interested in obtaining structural information, often the hydrogenated components are partially or totally replaced with the corresponding deuterated forms, which give rise to a lower level of incoherent scattering.

2.4 Specular reflection

In a reflectivity experiment a well collimated beam, which we will assume for the moment to be monochromatic, impacts under a certain angle θ_0 onto an interface that separates two different semi-infinite homogeneous media (0 and 1) and which we will initially assume as perfectly smooth. Similarly to what we know from optics, the beam is then partially reflected with an angle $\theta_r = \theta_0$ and partially refracted into the other medium, with an angle θ_1, as sketched in Figure 2.

The refraction is described by Snell's law, as for normal optics:

$$\frac{\cos\theta_1}{\cos\theta_0} = \frac{n_0}{n_1} \tag{6}$$

provided that we use the proper refractive index n for the two media. [3] For reasons of space, we will not go too much into the details of the quantum nature of neutron reflection at the interface. Here we limit ourselves to making some elementary observations on the neutron reflection process, which could be analyzed starting from Equation (5): in this Equation a (double) sum over the position of all the nuclei composing the sample has to be performed and this would require a detailed knowledge of the atomic structure of the sample. Luckily, we don't need such a level of detail and

[3] We mean that the refractive indices describing the reflection and refraction of the neutron beam have to be used. Their values are absolutely different and uncorrelated to the values that hold for optics.

a simplified approach may be adopted.

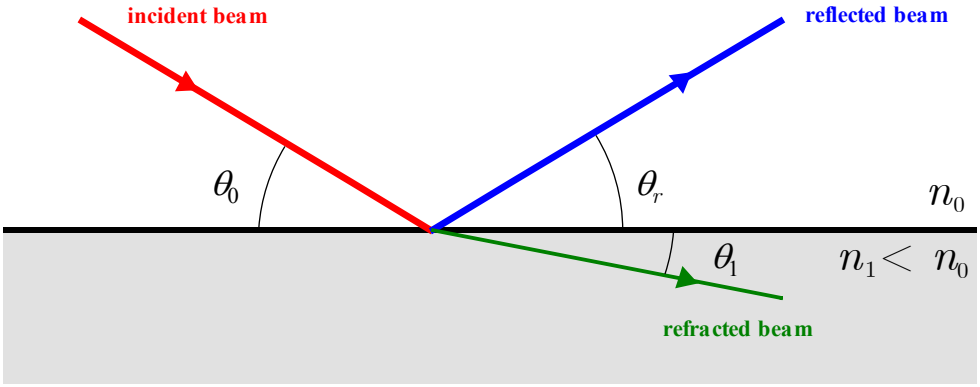

Figure 2 – Reflection and refraction from a smooth surface: θ_0 is the incident angle, whereas $\theta_r = \theta_0$ and θ_1 are the reflection and refracting angles, respectively. n_0 and n_1 indicate the refractive indices: in the figure $n_1 < n_0$, so the refracted beam bends outwards.

We start to observe that typical wavelengths of cold neutrons are much larger than the interatomic distances (usually in the order of an Ångström), which means that the potential that determines the characteristics of the scattering event is to some extent mediated over a certain number of atoms, rather that the single atom, ignoring the discontinuous structure of matter. This is mathematically equivalent to replacing the double sum with a double integral extended to the sample volume:

$$\left|\psi_{sc}\left(\vec{r}\right)\right|^2 = \frac{\left|\psi_0\right|^2}{r^2}\left\{\int_V \mathrm{d}^3 r \int_V \mathrm{d}^3 r' \rho\left(\vec{r}\right)\rho\left(\vec{r}'\right)\exp\left[-i\vec{Q}\left(\vec{r}-r'\right)\right]+\right.$$

$$\left.+\sum\nolimits_l N_l \left\langle \left(b_l - \left\langle b_l \right\rangle\right)^2 \right\rangle\right\}$$

where ρ is the so-called *scattering length density* (also indicated as *SLD*) which, inside a given volume V, can be evaluated as:

$$\rho = \frac{\sum_j b_j}{V} \tag{7}$$

where the sum is extended over all the atoms enclosed by the volume V.

The *SLD* plays an important role in neutron reflectivity experiments, as we will see in the following. For the moment we observe that, according to the hypothesis of homogeneity, each of the two media, 0 and 1, has a constant *SLD*, which we will indicate with ρ_0 and ρ_1, respectively.

The geometric and quantum-mechanical analysis of the neutron reflection at the interface as depicted in Figure 2 allows establishing that:

- in the case of specular reflection, the scattering vector $\vec{Q}$, defined by Equation (3), is perpendicular to the interface (the direction is usually referred to as the

z axis), its modulus being:

$$Q = Q_z = \frac{4\pi}{\lambda}\sin\theta_0 \tag{8}$$

This particular feature implies that with a reflectivity experiment we get information only on the structural arrangement in the direction normal to the interface

- the ratio n_1/n_0 between the two refractive indices may be written as:

$$\frac{n_1}{n_0} = \sqrt{1 - \frac{\lambda^2}{\pi}\left(\rho_1 - \rho_0\right)} \cong 1 - \frac{\lambda^2}{2\pi}\left(\rho_1 - \rho_0\right) \tag{9}$$

which shows, similarly to what we already know from optics, that the refractive index depends on the wavelength of the radiation used. The approximation used to get the rightmost term is based on the fact that the quantity $\lambda^2\left(\rho_1 - \rho_0\right)$ usually ranges from 10^{-6} to 10^{-4} for cold neutrons. Extending further the analogy, we can arbitrarily define the vacuum refractive index as unitary and in this way evaluate all (neutron) refractive indices with respect to it. Since for most of the isotopes the scattering lengths are positive, it can be immediately seen that in most cases, the refractive index of a medium will be less than one. This means that if we have a solid/air interface and if the neutron beam impinges onto the interface from the air (which practically has a null *SLD*) we should expect to observe the phenomenon of total reflection, provided that the incidence angle is below a certain critical value θ_c. To evaluate this angle it is sufficient to set $\theta_1 = 0$ in Equation (6) from which, using Equation (9), we obtain:

$$\theta_c \cong \lambda\sqrt{\frac{\rho_1 - \rho_0}{\pi}} \qquad\qquad \rho_1 > \rho_0 \tag{10}$$

It is important to note that although the critical angle of total reflection θ_c depends on the wavelength, the corresponding critical value of the scattering vector modulus Q_c is independent of it, as can be seen from combination of Equation (8) and (9):

$$Q_c = 4\sqrt{\pi\left(\rho_1 - \rho_0\right)} \tag{11}$$

In a reflectivity experiment, what is measured is the trend of *reflectivity* R as a function of the scattering vector modulus Q_z. The reflectivity R is defined as the ratio between the intensities of the reflected and incident beam. The solution of the wave equation to the interface of Figure 2 gives for R the result:

$$R = \left| \frac{Q_z - \sqrt{Q_z^2 - Q_c^2}}{Q_z + \sqrt{Q_z^2 - Q_c^2}} \right|^2 \tag{12}$$

In Figure 3 the calculated reflectivities are reported for the (smooth) air/Silicon interface ($\rho_{\mathrm{Si}} = 2.078 \cdot 10^{-6}\,\text{Å}^{-2}$): below the critical value Q_c the radiation sent on the sample is totally reflected and the reflectivity R is always unitary. However, the quantum-mechanical treatment based on the wave equation shows that, even in these conditions, the neutron has a non-zero probability to cross the interface and find itself in the medium with the lower refractive index: this is a typical example of the tunnel effect, very common for elementary particles. Above Q_c, neutrons have a progressively greater probability of crossing the interface and reflectivity values drop significantly. When $Q_z \gg Q_c$, reflectivities scale according to a power law of Q^{-4}. Since the reflectivity values spans several orders of magnitude, it is common to report R on a logarithmic scale, in order to better highlight the details of the trend as a function of Q_z. Figure 3 also shows what is the typical range of values of Q_z that is probed in reflexivity experiments, ranging from around 10^{-3} Å^{-1} to about 0.3 Å^{-1}.

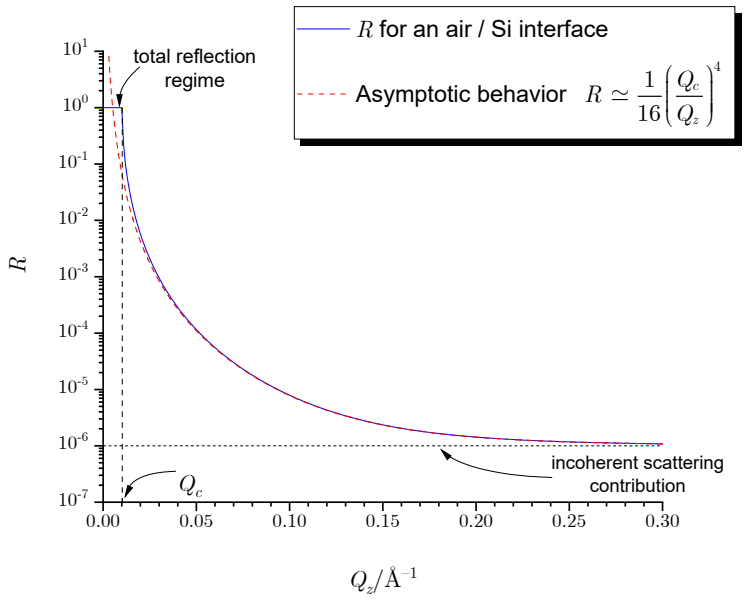

Figure 3 – Theoretical trend of reflectivity for an air/Silicon interface, as a function of the modulus of scattering vector. An intrinsic "background" value of $1 \cdot 10^{-6}$ has been assumed to realistically simulate the curve.

Although theoretically the reflexivity values should vanish for large Q_z values, this in practice is not observed both because of the presence of incoherent scattering and of the instrumental noise that make the reflexivity actually approaches to a constant non null value, although very small (usually of the order of 10^{-6}).

2.5 Reflectivity of a layered system

A layered system may be imagined as a stack composed of a certain number of different

media $\left(0,1,\ldots,n\right)$, each of which is characterized by a certain *SLD* value $\left(\rho_0,\rho_1,\ldots,\rho_n\right)$ and a thickness $\left(\tau_1,\tau_2,\ldots,\tau_{n-1}\right)$, with the first (0) and last (n) media assumed as semi-infinite. Similarly to what we treated in Section 2.4, the *SLD* distribution depends only on the direction z perpendicular to the various interfaces. Such a model describes appropriately many of the experimental systems studied with reflectometry (electrochemical systems, multi-material systems, biological membranes, etc.).

Application of quantum mechanics leads to expressing reflectivity with the recursive Parratt formalism. [7] Applying the condition according to which the wave function and its first derivative must be continuous at each interface, a series of recurrence relations is constructed from which it is possible to calculate the theoretical reflectivity as a function of Q_z: this reflectivity depends on the thickness of the layers, as well as on their composition (*SLD*). [4] Details of the formalism are beyond this short tutorial: here we will limit ourselves to demonstrating with elementary arguments, how the reflectivity trend depends on the superimposition of the neutron radiation reflected at the interfaces.

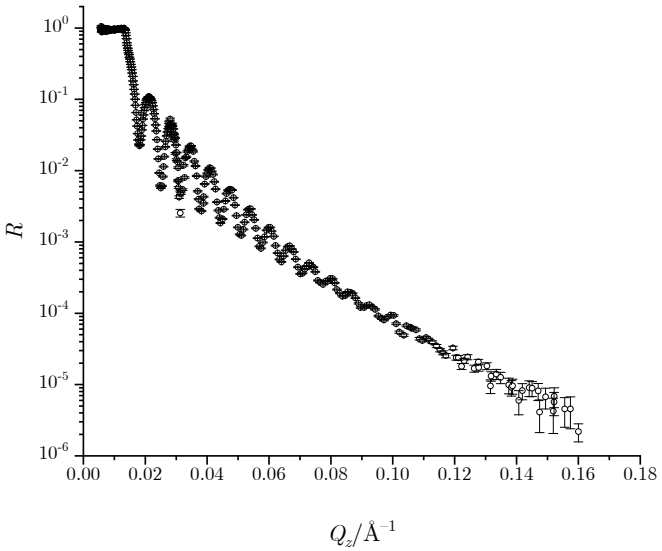

Figure 4 – Experimental reflectivities for a layered system with air/Titanium/glass interfaces as a function of the modulus of scattering vector, measured at REFSANS. The thickness of the intermediate Titanium layer is $\left(965 \pm 9\right)$ Å.

At this aim Figure 4 shows the experimental reflectivities measured on a glass sample ($\rho_{\text{glass}} = 3.808 \cdot 10^{-6}\,\text{Å}^{-2}$) coated with a thin Titanium layer (about 100 nm thick, $\rho_{\text{Ti}} = -1.949 \cdot 10^{-6}\,\text{Å}^{-2}$). Differently from what seen in Figure 3, here above the critical angle of total reflection the presence of a certain number of interference maxima and minima are present. These interference fringes are called *Kiessig fringes*, from the name of the scientist Heinz Kiessig who first observed them in 1931. [8]

The position of the Kiessig fringes is strictly connected to the interference occurring

[4] An equivalent approach has been developed by Abeles, which uses a matrix formalism.

between the neutrons reflected at the air/Titanium and Titanium/glass interfaces, as shortly sketched in Figure 5. To have a maximum of interference at a certain Q_z value, the difference in the optical path between reflected radiation at the two interfaces must be equal to an integer number N of wavelengths. From trivial geometric considerations it is possible to see that this happens only when:

$$Q_z \cong \frac{2\pi}{\tau_1} N \qquad\qquad N \in \mathbb{N} \tag{13}$$

similar to the Bragg's law studied in crystallography. Equation (13) shows how the interference phenomena in reciprocal space are connected to the length scales.

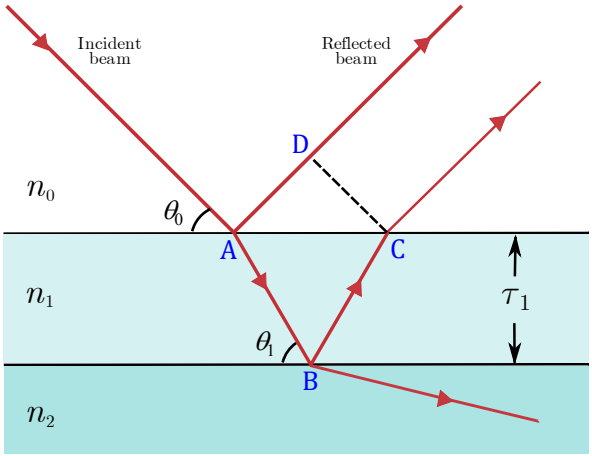

Figure 5 – Superimposition of reflected waves generated at the different interfaces. The optical path difference is given by the quantity $\overline{\mathrm{AB}} + \overline{\mathrm{BC}} - \overline{\mathrm{AD}}$.

2.6 Roughness

So far we have always assumed that all interfaces were perfectly smooth surfaces. It is quite easy to guess that on an atomic scale this is not true at all, and that even in the presence of a system similar to a multilayer, all interfaces always show a certain degree of roughness. This fact leads to some very important consequences, the most obvious of which is that in addition to the specular reflection, there will be a certain amount of neutrons that will be reflected in *off-specular* conditions. Very often the amount of this phenomenon is very small compared to specular reflection but nevertheless it is a symptom of how far the interface is from the conditions of a perfect geometric plane.

For a real interface, the refractive index no longer depends only on the perpendicular coordinate z at the interface but also on the parallel ones x and y. To take into account such a dependence we would need to know the real form of the interface described in a general way by a function $z\big(x,y\big)$. However, this level of detail is actually completely useless: what we need for an effective description of surface roughness is a statistical approach. If we suppose, in fact, that the deviation of the surface from the ideal smooth configuration has a random distribution, the probability $P\big(\Delta z\big)$ that at a certain point of the surface the interface is higher or lower of Δz with respect to the average is

described by a Gaussian function (see Figure 6):

$$P\left(\Delta z\right) = \frac{1}{\sqrt{2\pi\sigma^2}} \exp\left[\frac{-\left(\Delta z\right)^2}{2\sigma^2}\right] \tag{14}$$

and the profile of the refractive index $n\left(z\right)$ at the interface between the media i and $i+1$ is:

$$n\left(z\right) = \frac{n_i + n_{i+1}}{2} - \frac{n_i - n_{i+1}}{2} \operatorname{erf}\left(\frac{\Delta z}{\sqrt{2\sigma^2}}\right) \tag{15}$$

where σ represents the *roughness* of the interface between the media i and $i+1$, and erf is the error function. Thus the roughnesses of all the interfaces are important and for a correct quantitative analysis they have to be included in the Parratt approach. This leads to the appearance of a damping factor which reduces the depth of the oscillations in the reflexivity pattern, as depicted in Figure 7.

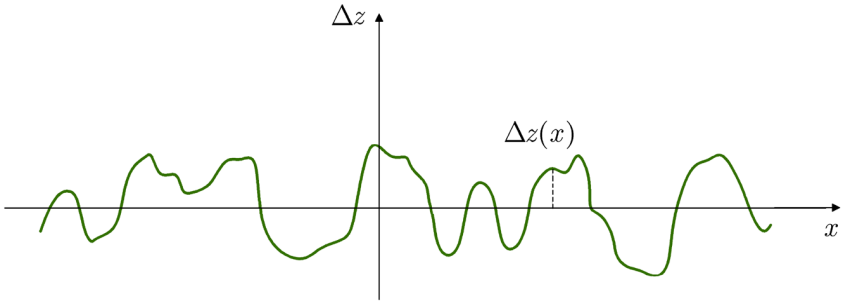

Figure 6 – Sketch of the roughness of a real interface. For simplicity, only the dependency along a direction is shown. The horizontal axis (x) is placed at the average level of the interface

2.7 The REFSANS reflectometer

In order to get a reflectivity pattern, like the one shown in Figure 4, we have to measure the reflectivities R at different values of Q_z. According to Equation (8) we may either select a certain neutron wavelength and measure R at different incident angles, or select a suitable value of the incident angle and use neutrons of different wavelengths. The first approach is often adopted at nuclear reactor sources, where because of the continuous flux coming from the source, neutrons with a certain wavelength are selected (by means of a velocity selector) and their incident angle is changed to get the Q_z dependence.

At a spallation source, a pulsed “white” beam is sent on the sample and the angle is constant (or at most limited to a small number of different values). The neutron wavelength is evaluated by measuring the time Δt required to fly from a certain reference point to the detector, whose distance is D: in this way we have access to the neutron speed that we can correlate to its wavelength through de Broglie's equation:

$$\lambda = \frac{h}{mv} = \frac{h}{mD}\Delta t \tag{16}$$

This technique is typical of the so-called *time-of-flight* instruments.

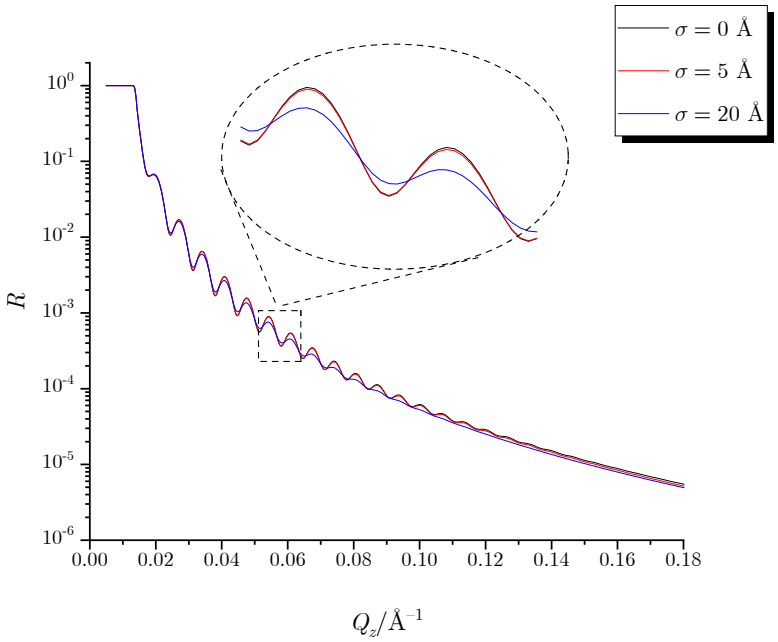

Figure 7 – Theoretical trend of reflectivities for a layered system with air/Titanium/glass interfaces for different values of the air/Titanium interfacial roughness. The inset highlights the different trends.

Actually, the use of time-of-flight reflectometers is not limited only to spallation sources: even in continuous sources, such instruments are necessary if, for example, we want to measure reflectivities from liquid-gas interfaces. In this case for obvious reasons the surface is horizontal and the only advantageous way to have access to a wide range of Q_z values is to use an incident polychromatic beam, tilting the incident beam to a small set of angle values. Another very important advantage of time-of-flight instruments concerns the possibility to have access to a large Q_z range with a single incident angle, very important for investigations of kinetic phenomena occurring at interfaces.

For the experiment planned for this tutorial, the time-of-flight instrument REFSANS will be used. REFSANS is the horizontal reflectometer with GISANS option operated by Helmholtz-Zentrum Hereon at the Heinz Maier-Leibnitz Zentrum (MLZ) in Garching. [9] It has been conceived to measure both specular and off-specular reflectometry for solid/liquid, solid/gas, and liquid/gas interfaces.

Figure 8 shows a sketch of REFSANS. The instrument consists of three pairs of chopper disks to define the wavelength resolution and wavelength band, a collimation system and optical components which are able to bend, if necessary, the incident beam. The neutrons are recorded by a 2-D detector, which can be lifted by up to 5 deg.

Typical reflectometry curves are recorded using two or three incident angles to cover

the range $0.005 \leq Q_z \big/ \text{Å}^{-1} \leq 0.25$.

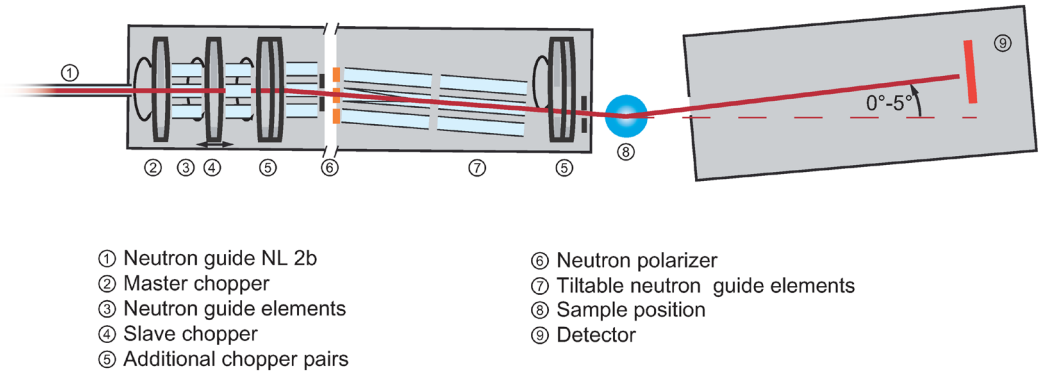

Figure 8 – Sketch of REFSANS as seen from the side.

3 Preparatory exercises

The following questions will be useful during your experiment on REFSANS, so it is highly recommended that you answer them before starting the experiment, in order to get a clearer picture of what you will be doing.

1. Try to prove Equation (13). Help yourself with Figure 5. During the derivation some approximations are necessary: for this purpose keep in mind that the refractive indices of the various media are numbers that differ by less than one part in ten thousand from the unit.

2. We have stated that REFSANS is an instrument working in time-of-flight mode. The horizontal distance between the first chopper disk and the detector can reach 21.5 m when the detector is placed at the maximum possible distance from the sample. Try to estimate the time-of-flight between these two points. Perform such evaluation for the fastest and slowest neutrons typically used at the instrument, namely $\cong 2$Å and $\cong 21$Å. All the necessary fundamental physical constants may be found on the NIST website. [10]

3. The duration of a neutron pulse cannot be shorter than the interval of time required for the fastest and slowest neutrons to reach the detector. Based on the estimations performed in the previous point, try to estimate at which rotational speed (expressed as revolutions per minute, rpm) the chopper disks can be rotated to provide the wavelength band $2 \leq \lambda \big/ \text{Å} \leq 21$.

4. When a pulse starts, the neutrons inside the region enclosed between the first and second disk (master and slave choppers, respectively; see Figure 8) travel towards the sample and then towards the detector. It is normally assumed that the uncertainty affecting the measurement of the time-of-flight is negligible (indeed it is really small, being some hundreds of nanoseconds). Based on this assumption,

what can be said about wavelength uncertainty?

5. The neutron beam has to be collimated in order to define its direction as precise as possible. Figure 9 shows the most used principle used to collimate a beam: a system composed of two slits. The dashed line represents the path of an ideal infinitely collimated beam, whereas the solid lines the effective divergence. The uncertainty on the angle that the beam forms with the sample is given by $\Delta\theta$, as represented in the figure. If the vertical apertures of the slits are b_1 and b_3, and if the distances between the slits is l, show that the angular uncertainty $\Delta\theta$ is given by:

$$\Delta\theta = \arctan\frac{b_1 + b_3}{2l} \tag{17}$$

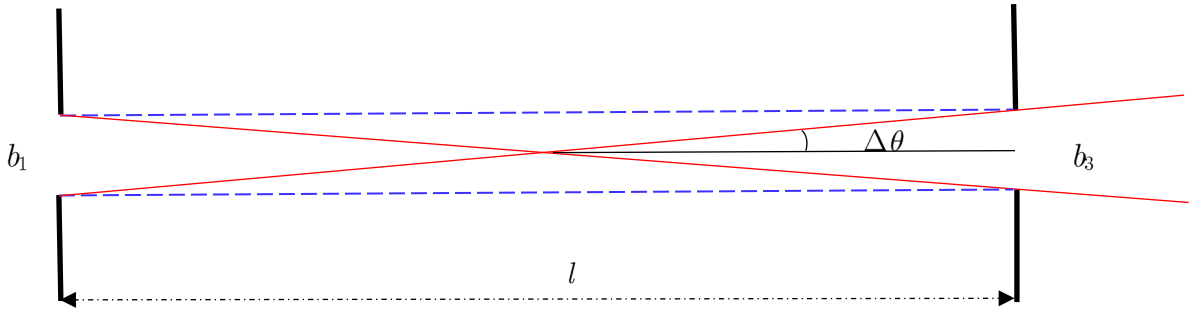

Figure 9 – Principle of the REFSANS collimation system, from a lateral view

6. Because of the time-of-flight mode, at REFSANS it is possible to cover a large Q_z range with a single angle of incidence. In case a wavelength band of $2 \leq \lambda/\text{Å} \leq 21$ is used, try to evaluate the Q_z range covered if the neutron incident angles are 0.50 deg and 2.50 deg. How can the incident angles be set?

4 Experiment procedure

In the experiment you are about to start, a Silicon block coated with a layer of Titanium and an additional layer of Aluminum will be measured, to get information about the thickness and the quality of the coating layers. The two metallic layers have been deposited through the sputtering technique. [11]

Blocks like the one to be tested can be used as electrode in an electrochemical cell, to study corrosion phenomena occurring at the surface: the Aluminum surface is put in contact with a corrosive liquid and counter/reference electrodes. Then the Al/liquid interface is probed by neutron reflectivity. During the experiment, the potential between the electrodes or a certain current may be imposed through the use of a potentiostat/galvanostat.

This is a typical description of a so-called "*in-operando*" experiment: an experiment

where a certain phenomenon is promoted imposing some quantities (such as the electrical current), and is investigated during its occurrence, at its site (*"in-situ"*).

In our experiment we will limit ourselves to simply investigate the surface of the block: for investigations with neutron reflectometry, and even more so for electrochemical experiments, it is important that the surface is as smooth as possible to prevent the occurrence of off-specular scattering and low reflectivity.

4.1 The experiment itself

A short overview of REFSANS will take place, and the main characteristics of the TOF-analysis will be shortly discussed.

A Silicon block with Ti/Al layers will be provided. The thicknesses declared by the manufacturer are $\tau_1 = 100$Å for the Titanium layer and $\tau_2 = 500$Å for the Aluminum layer. Some of you will mount the block over a cell holder and install it at the instrument. After a short discussion about the order of the interfaces to be probed, the sample will be aligned.

To cover a Q_z interval ranged between $6 \cdot 10^{-3}$ Å^{-1} and 0.15 Å^{-1} we will use the a wide wavelength range (from 2 to 21 Å) and two incident angles, namely 0.50 deg and 2.50 deg. After a short discussion on the beam size to use and on the detector position, the measurement will be started. The measurement times can be set as 20 min for the primary beam, 40 min for the low angle measurement, and 2.5 h for the 2.50 deg measurement.

4.2 Data reduction

The data reduction will be performed with the instrument scientist, who will explain the fundamental steps and provide the reflectivity, R, *vs.* the vertical component of the momentum transfer, Q_z.

4.3 Data evaluation

Data evaluation of the measured reflectivities strongly depends on the system under investigation. For a simple system composed of a single interface or two interfaces, some of the characteristics may be obtained through a simple analysis of the pattern, such as position of maxima, distance between two consecutive maxima, position of the critical angle, etc.

For more complex systems, or even for gaining more details on simple systems, a full analysis of the results has to be performed. If the system can be described as a layered system, reflectivities may be analyzed through the Parratt recursion algorithm, as mentioned in Section 2.5. [7] Many programs are available for the analysis of reflectivity data. One good example is Motofit, [12] a package working in the IGOR Pro environment. [13] Motofit co-refines neutron reflectometry data, using the Abeles matrix formalism and least squares fitting. Other valid alternatives are Parratt32, formerly developed at the BErlin Neutron Scattering Center (now known as Helmholtz-Zentrum Berlin), and

GenX. [14]

The programs ask for the number of layers existing in the system to be analyzed, their SLD, thickness and roughness of the interfaces.

5 Experiment-Related Exercises

1. Observe the reflectivity data and try to qualitatively determine the main characteristics.
2. Try to list all the uncertainties that lead to an error on the evaluation of Q_z and propose a formula for an estimation of such an error.
3. The mass density of Aluminum, Silicon and Titanium at room temperature are $2.699\,\mathrm{g}/\mathrm{cm}^3$, $2.336\,\mathrm{g}/\mathrm{cm}^3$ and $4.506\,\mathrm{g}/\mathrm{cm}^3$, respectively. Try to estimate the scattering length densities (SLD) of such elements. Try also to estimate the SLD of air, in normal conditions. Scattering lengths may be found on the NIST webpage.[15] Try to list all other information you need to perform the requested estimation.
4. For the neutron reflection between two semi-infinite slabs, the critical value of Q_z is given by Equation (11), $Q_c = 4\sqrt{\Delta\rho \cdot \pi}$, where $\Delta\rho$ is the difference between the scattering length density (SLD) of the two media. Try to compare this theoretical value with the experimental one observed.
5. Try to make an approximate sketch of the trend of the SLD *vs.* the vertical distance from the interface Si/Ti. How do you expect the SLD to change across the various interfaces?
6. The maxima and minima are due to the presence of the Aluminum and Titanium layers, which influence the neutron wave exercising a different potential and creating the conditions for constructive interference along proper directions. Thus, the position of the maxima depends on the (constructive) interference occurring between the neutron waves reflected from the different layers. A (broad) maximum at high Q_z should correspond to the thinner layer (Ti): therefore, its position should give a very rough estimation (at least as order of magnitude) of the Ti layer. Try to use the Bragg equation to estimate if the corresponding thickness agrees with the expected value. Also, discuss why this estimation might not give a proper value for the thickness.
7. Assume to have installed Motofit, to perform a full analysis of the reflectivity data. The program starts with a simple three-interface system, namely Air/SiO_2/Si: a thin layer of SiO_2 ($SLD = 3.475 \cdot 10^{-6}\,\text{Å}^{-2}$) is always present on top of Si substrates. The roughness of the Si surface is, according to the manufacturer, ranged between 5 and 10 Å. Set 10 Å as starting value for this interface. Set also 15 Å as thickness for the SiO_2 layer. Afterwards the total

number of layers have to be defined: in principle, besides the SiO_2, Ti, and Al layers, an additional layer of Al_2O_3 and, possibly, a layer of TiO_2 should be added on top of the correspondent metallic layers. Anyway, since these layers are most likely very thin (< 2-3Å), they can be neglected for a first analysis. Thus, add the layers of Al and Ti along with the *SLD* evaluated in Section 2 and the expected thicknesses. Also set a value of 9% for $\Delta Q_z / Q_z$ and try to fix all the values except the thicknesses of the Al and Ti layers. Fit and judge the fitting. Roughness smears the minima and maxima: try to leave free the roughness for the Ti, Al and SiO_2 interfaces and re-fit. Finally, if the fitting is not satisfactory, try to leave free the *SLD* of the two metallic layer and judge the re-fitting. Try also to understand if some values are different from those expected and why.

8. As general rule, for reflectivity investigations, the roughness should not exceed 10 to 15 Å. Based on the results obtained, try to judge the quality of the layers sputtered on the Silicon crystal.

6 References

[1] Daillant, J.; Gibaud, A., *X-ray and neutron reflectivity : principles and applications*. 2nd ed.; Springer: Berlin, 2009; p xiv, 348 p.

[2] REFSANS - Large scale structures - Instruments & Labs - MLZ - Heinz Maier-Leibnitz Zentrum. https://www.mlz-garching.de/refsans.

[3] Marshall, W.; Lovesey, S. W., *Theory of Thermal Neutron Scattering*. Oxford Clarendon Press: 1971.

[4] Sivia, D. S., *Elementary scattering theory : for X-ray and neutron users*. Oxford University Press: Oxford ; New York, 2011; p xii, 201 p.

[5] Higgins, J. S.; Benoît, H. C., *Polymers and Neutron Scattering*. Oxford Clarendon Press: 1996.

[6] Levine, I. N., *Quantum chemistry*. Seventh edition. ed.; Pearson: Boston, 2014; p 700 pages.

[7] Parratt, L. G., Solid Surface Studies by Total Reflection of X-Rays. *Physical Review* **1954,** *95* (2), 617-617.

[8] Kiessig, H., Interferenz von Röntgenstrahlen an dünnen Schichten. *Annalen der Physik* **1931,** *402* (7), 769-788.

[9] Moulin, J.-F.; Haese, M., REFSANS: Reflectometer and evanescent wave small angle neutron spectrometer. *Journal of large-scale research facilities JLSRF* **2015,** *1* (A9), 1-3.

[10] Mohr, P. J.; Newell, D. B.; Taylor, B. N. Fundamental Physical Constants from NIST. https://physics.nist.gov/cuu/Constants/.

[11] Stuart, R. V., *Vacuum technology, thin films, and sputtering : an introduction*. Academic Press: New York, 1983; p viii, 151 p.

[12] Nelson, A. Motofit and Reflectometry (scattering) resources Wiki. http://motofit.sourceforge.net/wiki/index.php/Main_Page.

[13] Wavemetrics Inc., IGOR Pro 6.3 Download Links. https://www.wavemetrics.com/order/order_igordownloads6.htm.

[14] Björk, M.; Glavic, A. GenX - Home. https://genx.sourceforge.io/.

[15] NIST Center for Neutron Research, Neutron scattering lengths and cross sections. https://www.nist.gov/ncnr/planning-your-experiment/sld-periodic-table.

7 Contacts

REFSANS

Phone: +49-89-289-14880; +49-89-158860-550

Web: https://mlz-garching.de/refsans

Jean-François Moulin

Helmholtz-Zentrum Hereon

German Engineering Material Science am Maier-Leibnitz Zentrum.

Lichtenbergstraße 1, D-85747 Garching

Phone: +49-89-158860-762

e-mail: Jean-Francois.Moulin@hereon.de

Gaetano Mangiapia

Phone: +49-89-158860-839

e-mail: Gaetano.Mangiapia@hereon.de

Martin Haese

Phone: +49-89-158860-763

e-mail: Martin.Haese@hereon.de

Engineer

Matthias Pomm

Phone: +49-89-158860-761

e-mail: Matthias.Pomm@hereon.de